COBEM 2023 27TH INTERNATIONAL CONGRESS OF MECHANICAL ENGENEERING

ABCM Brazilian Society of Mechanical Sciences and Engineering
27th ABCM International Congress of Mechanical Engineering
December 04-08, 2023, Florianópolis-SC, Brazil

COB-2023-1546
NUMERICAL DEVELOPMENT OF A PASSIVE HEAT EXCHANGER FOR ELECTRIC VEHICLE BATTERIES USING PHASE CHANGE MATERIAL (PCM)

Luis Gonçalves da Silva Junior
Guilherme Borges Ribeiro
Applied Thermal Engineering Laboratory, Aeronautics Institute of Technology – ITA, São José dos Campos, Brazil
luis.junior.101263@ga.ita.br
guilherme.ribeiro@gp.ita.br

Abstract. *This study focuses on the development of electric vehicles, where batteries play a significant role. Over the years, improvements in battery technology have been made, focusing on parameters such as weight, storage, and operating temperature. This latter aspect is a crucial factor affecting battery performance, lifetime, and safety, making it necessary to have an effective thermal management system to control temperature setpoint and reduce peak temperature. In this regard, the use of phase change material (PCM) as a passive technique is a promising technique to efficiently establish the thermal management system without additional power consumption. The objective of this work is to numerically analyze a new heat exchanger model for electric vehicles with a heat sink coupled to the PCM. Key results include that the presence of the finned heat sink in the heat exchanger proved to be efficient, considering that the presence of several zones with boundary layer development provided heat transfer intensification mainly where these phenomena were more evident. The presence of a larger number of fins in the heat exchanger reduced the performance of the equipment over time in relation to the thermal storage capacity and the mass of molten liquid produced.*

Keywords: *Phase Change Material, Computational Fluid Dynamics, Heat transfer, Battery Thermal Management Systems*

1. INTRODUCTION

Since the industrial revolution the emissions of pollutants linked to fossil fuels have been increasing considerably because with the great industrial rise, more and more energy resources were needed to meet the demand required with the need to follow the technological growth not only from the industrial point of view but also the evolution of the population that began to migrate to large cities and consume more energy, whether for cooking, heating or transport. However, the emission of pollutant gases is inherent to global warming and the greenhouse effect, which are responsible for the climate changes that we can already notice the consequences, for example, rising sea levels, shrinking glaciers, heat waves, etc (Helbling & Meierrieks, 2022). The transport sector is approximately 95% dependent on fossil fuels and is the largest contributor to air pollution (Bicer & Dincer, 2017), directly producing emissions of carbon monoxide, nitrogen dioxide and other hydrocarbons linked to the combustion process. In this sense, electric vehicles emerge as a potential player to reduce greenhouse gas emissions and become a zero-emission and carbon-neutral means.

Electric vehicles have been the focus in recent years as a synonym for efficient and sustainable mobility. Despite not being a very recent technology, high costs and lack of technology were difficulties encountered in the past for the evolution of this type of vehicle. The concern for low-emission sources and the advances in recent years have been changing the scenario for electric vehicles, especially in the more developed countries with the concern to reduce the dependence on oil and gas from fossil resources. However, batteries are still a major challenge for electric vehicles, both in terms of energy storage capacity and the weight attached to the systems in order to ensure a good range for the vehicle. Currently, lithium-ion batteries (LIBs) are the market leaders due to their better energy density, good life cycle, rechargeability, and safety (Liu et al., 2022). The battery thermal management system is one of the key systems to ensure that the battery is functioning well, as the operating temperature of the battery can be a problem if it is too hot or too cold. Temperature is very important for maintaining the life, performance, and safety of the batteries. Under high-temperature environments, lithium-ion batteries may produce thermal runaway, resulting in short circuits, combustion, explosion, and other safety problems (Zhang et al., 2022). There are two crucial factors of good features of a thermal management system for batteries, the first is to avoid thermal runaway phenomena and the second is to reduce temperature peaks (Pesaran et al., 1999).

Battery thermal management systems can be divided into two categories passive and active. The active system has low heat exchange efficiency and some limitations when the battery works in abusive situations, can not guarantee a good

temperature uniformity in the battery, in addition, it requires a lot of equipment to be able to handle all the thermal load, for example, pumps, ducts, heat exchangers, and compressors. In the passive category, Phase Change Materials (PCM) have emerged as an efficient way to ensure a more comfortable thermal behavior for batteries without the need for additional equipment and without consuming energy (Javani et al., 2014). Phase change materials (PCMs) absorb or release a large amount of latent heat during the process of transforming physical properties. Using them together with the battery improves the heat transfer process from the battery to the passive heat exchanger, and because the PCM can absorb large amounts of heat, it helps to maintain the temperature of the battery more uniformly. PCMs can even be used in conjunction with an active system to control the temperature, but the active system may be reduced (Luo et al., 2022). Mohammad *et al.* analyzed different PCM configurations coupled to a lithium-ion battery and achieved an average of 6 K reduction in battery temperature (Heyhat et al., 2020).

Although the use of PCM is still scarce, it is essential to develop new research to enhance the application of this material in line with the development of new technologies for electric vehicles. The objective of this work is to numerically analyze a new heat exchanger model for electric vehicles with a heat sink coupled to the PCM. The numerical model, developed and solved with Ansys Fluent 22R2, includes equations of conservation of mass, momentum, and energy. The fluid domain was designed as a bi-dimensional cartesian model to represent the physics of the problem coherently and reduce computational cost. A parametric analysis will be presented with three heat sink fin configurations to evaluate the variation of melting time and material temperature over time. The critical dimensionless parameters for this analysis will also be identified. The main objective is to assess the heat absorption capacity over time, evaluate the performance of the conjugate heat transfer between the heat sink and the fluid domain of the PCM and analyze the best performance of the exchangers in view of a thermo hydraulic analysis of the process.

2. COMPUTATIONAL METHODOLOGY

Although many studies in the literature present the material melting process as a fluid without the influence of buoyancy, the gravitational effects are extremely important because they can considerably modify the melting time of the material and the flow profile due to the effects of natural convection. Thus, in this study the flow was modeled as incompressible, Newtonian, transient and laminar due to the low Grashof number (Gau & Viskanta, 1986). ANSYS Fluent was the commercial software used to solve the numerical model and the melting process of the material using the enthalpy-porosity technique (Voller & Prakash, 1987). In this technique, the melt interface is not tracked explicitly. Instead, a quantity called the liquid fraction, which indicates the fraction of the cell volume that is in liquid form, is associated with each cell in the domain. The liquid fraction is computed at each iteration, based on an enthalpy balance. The mushy zone is a region in which the liquid fraction lies between 0 and 1. The mushy zone is modeled as a "pseudo" porous medium in which the porosity decreases from 1 to 0 as the material solidifies. When the material has fully solidified in a cell, the porosity becomes zero and hence the velocities also drop to zero (Voller & Prakash, 1987).

The continuity equation solved in the full domain is given by:

$$\frac{\partial \rho}{\partial t} + \nabla \cdot (\rho \boldsymbol{u}) = 0 \tag{1}$$

Where ρ is the fluid density and **u** is the fluid velocity vector. The mushy zone is modeled assuming a mushy fluid model in which the solid and fluid velocities are equal in the mushy zone (Voller et al., n.d.). The momentum conservation equation solved in the full computational domain is:

$$\frac{\partial}{\partial t}(\rho \boldsymbol{u}) + \nabla \cdot (\rho \boldsymbol{u}\boldsymbol{u}) = -\nabla p + \nabla \cdot \sigma + \rho g + S \cdot \boldsymbol{u} \tag{2}$$

In fully solidified regions, the porosity is equal to zero, which extinguishes the velocities in these regions. The momentum source due to the reduced porosity in the mushy zone takes the following form:

$$S = \frac{(1-\beta)^2}{(\beta^3 + \varepsilon)} A_{mush} \tag{3}$$

Where β is the liquid volume fraction, ε is a small number (0.001) to prevent division by zero, A_{mush} is the mushy zone constant defined as 10^6 for this paper, because it is where the melt interface curvature of lauric acid correlates well with experimental results.

The PCM is in the fluid phase above the temperature T_l, in the mushy phase between T_s and T_l, and in the solid phase below T_s. Considering a temperature-range for phase change in the PCM, the liquid melt fraction, β, is defined to vary linearly with temperature with $T_s \leq T \leq T_l$ (Mallya & Haussener, 2021):

$$\beta = \frac{(T - T_s)}{(T_l - T_s)} \tag{4}$$

The enthalpy of the material is computed as the sum of the sensible enthalpy h, and the latent heat, ΔH:

$$H = h + \Delta H \tag{5}$$

Where,

$$h = h_{ref} + \int_{T_{ref}}^{T} c_p dT \tag{6}$$

The h_{ref} is the reference enthalpy, T_{ref} is the reference temperature and c_p is the specific heat at constant pressure. The latent heat content can be written in terms of the latent heat of the material, L:

$$\Delta H = \beta L \tag{7}$$

The latent heat content can vary between zero (for a solid) and (for a liquid). Thus, for solidification/melting problems, the energy equation is written as:

$$\frac{\partial}{\partial t}(\rho h) + \nabla \cdot (\rho \boldsymbol{u} h) - \nabla \cdot (k \nabla T) = 0 \tag{8}$$

A second-order upwind discretization scheme was used to solve the momentum and energy equations; the PRESTO scheme was selected for the pressure correction equation; and the semi-implicit method for pressure-linked equations (SIMPLE) algorithm was used for the pressure–velocity coupling. The time step is 0.05 s, with a maximum of 200 iterations being performed along the entire domain for each time step. The convergence criterion for the scaled residuals was set to 10^{-4} for continuity equation, 10^{-5} momentum equation, and 10^{-8} for energy equation, as recommended by previous research (Zeng et al., 2017).

2.1 Physical properties

The Lauric Acid were used based on the experimental studies by Kamkari et al.(Kamkari et al., 2014; Shokouhmand & Kamkari, 2013). One of the main characteristics of this material is the high Prandtl number (Pr = 137). Table 1 shows the thermophysical properties of the material. The density, viscosity and conductivity were modeled according to the temperature variation to approximate the experimental results with the numerical using a piecewise-linear function within the ANSYS Fluent.

Table 1. Thermophysical properties of lauric acid (Shokouhmand & Kamkari, 2013)

Specific heat capacity solid/liquid (kJ/kg K)	2.18/2.39
Melting temperature range (K)	316.65/321.35
Latent heat of fusion (kJ/kg)	187.21
Density solid/liquid (kg/m^3)	$\frac{885}{0.001(T - T_l) + 1}$

The density's dependency on temperature is expressed with Boussinesq model, which simplifies the change in density using a thermal expansion coefficient γ. The thermal expansion coefficient γ is 0.001 K^{-1}, which is calculated based on volume expansion measured in experiments (Zeng et al., 2017).

$$\rho = \frac{\rho_l}{\gamma(T - T_l) + 1} \tag{9}$$

Where, ρ_l (kg/m^3) is the density of liquid PCM at the phase change temperature T_l, in K.

The dynamic viscosity, μ_l ($\frac{Kg}{ms}$) was also modeled as a function of temperature and can be represented by the following polynomial:

$$\mu_l(T) = 3x10^{-6}(T^2) - 0.0005(T) + 0.0242 \tag{10}$$

Finally, the thermal conductivity can be modeled according to table 2.

Table 2. Variation of thermal conductivity of the lauric acid with temperature (Shokouhmand & Kamkari, 2013).

Temperature (K)	293	303	313	323	328	333	338	343
Thermal conductivity (W/m K)	0.161	0.159	0.158	0.145	0.143	0.142	0.139	0.138

In this paper the non-dimensional Rayleigh and Nusselt numbers are studied in order to better understand the characteristics of the phenomena. The Rayleigh number, Ra_y (Equation 11), compares the time scale for conduction and convection, i.e. the ratio of viscous and buoyant forces. The Nusselt number, Nu_y, (Equation 12) is a measure of the instantaneous heat transfer rate expressed as ratio between total and conductive heat transfer. The characteristic length of the non-dimensional numbers, y, is the height, in a vertical configuration.

$$Ra_y = \frac{g\beta(T_w - T_m)y^3}{\nu\alpha} \tag{11}$$

Where, g is the acceleration due to gravity (9.81 m s^{-2}), T_w is the solid temperature, T_m is the PCM temperature, y is the vertical height, ν is the kinematic viscosity (m^2 s^{-1}) and α is the thermal diffusivity (m^2 s^{-1}).

$$Nu_y = \frac{\dot{q}}{(T_w - T_m)}\frac{y}{k_l} \tag{12}$$

Where, $\dot{q}$ is the heat flux (Wm^{-2}) and k_l is the liquid PCM conductivity (Wm^{-1} K^{-1})

2.2 Numerical validation

In order to validate the numerical model, a validation study was carried out based on the experimental study performed by Kamkari et al. (Kamkari et al., 2014). Although in the experimental study the geometry is three-dimensional, the authors made a cut in the middle of the geometry to acquire the simulation results, so in this study a two-dimensional geometry was used since the case can be physically represented in this way. The geometry used in the numerical study has a height of 0.12 m and a length of 0.05 m, the same configurations used in the cross section of the experiment. The boundary conditions used in both the experimental and numerical studies consist of a constant temperature of 343.15 K on one vertical wall, while the other walls have an adiabatic condition. A fully structured mesh with perfect orthogonal quality with 10000 elements was generated in order to correctly capture the physical phenomena and reduce discretization errors in the model. Figure 01 illustrates the dimensions of the computational domain, the boundary conditions and the mesh.

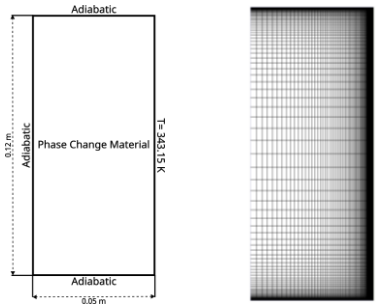

(a) (b)

Figure 1. Computational domain, boundary conditions, and mesh.

The results show a good prediction of the simulation with the experimental results and with the numerical result from Zeng et al. (Zeng et al., 2017) as shown in figure 02.

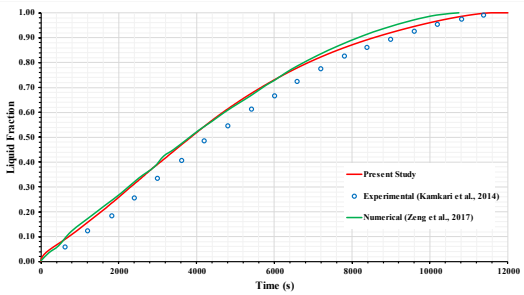

Figure 2. Numerical and experimental results of liquid fraction over the time.

A simulation of approximately 180 min of physical time was performed in order to analyze the almost complete melting of the material. Thus, we can consider that the physical phenomenon is being well represented numerically by the computational model and generate new geometric configurations to explore the behavior of the material melting process.

2.3 Battery System

The present work was developed with the focus on creating a passive system heat exchanger to assist in the performance of the cooling process of the battery pack of the i3 vehicle developed by BMW Group (Schoewel & Hochgeiger, 2014). Table 3 illustrates some characteristics of the battery system of this electric vehicle. Currently, the battery cooling system is coupled with the air conditioning system itself, a fact that considerably reduces weight, as it eliminates additional equipment. The use of an auxiliary heat exchanger aims to improve the cooling efficiency of the batteries and ensure greater safety and life cycle, since it will help to avoid large temperature peaks.

Table 3. BMW i3 battery pack technical data (Schoewel & Hochgeiger, 2014).

Nominal voltage	360 V
Maximum current	409 A
Energy content	22 kWh
Discharge Power peak	147 kW
Weight	233 kg

One of the great challenges in adding new equipment to electric vehicles is not to significantly change the weight of the vehicle, as the weight of the battery is currently still a challenge to be overcome by engineering with new technologies more efficient. Thus, it becomes prohibitive to add any equipment to the vehicle that significantly changes the weight. In this study, in addition to the weight, the space for the coupling of the heat exchanger is restrictive, as there is no useful space inside the battery pack and the coupling of the PCM directly into the cells is unfeasible due to the non-cylindrical shape of the cells of this vehicle, in addition to the safety factor linked to the direct coupling of a material that can be flammable to the detriment of a direct spark without protections. Figure 3 illustrates the battery pack of the BMW i3.

Figure 3. BMW i3 battery pack (Schoewel & Hochgeiger, 2014).

2.4 Computational domain

With the intent of taking advantage of the useful space available in the external battery casing, the heat exchanger was designed to operate within a dimension of 1.4 m length, 0.11 m width and 0.15 m height. Due to the space and weight limitations in the vehicle for the coupling of a passive cooling system, in the present study the coupling of a heat sink is used in order to intensify the heat transfer from the battery pack to the passive system. The dimensions reserved for the coupling of the system are preserved, and as seen in the validation process, a simplification to a two-dimensional model is possible in order to reduce the computational cost of the simulation. Therefore, the heat sink geometry was generated coupled with the fluid domain to allow a conjugate heat exchange. In this work three heat sink models are analyzed with different fin configurations, the first with five fins with a length of 0.02 m, the second with 5 fins with a length of 0.04 m, and the third with 10 fins with a length of 0.04 m. Due to weight restrictions and good thermal conductivity, aluminum was the material used in the heat sink solid and the table 4 illustrates the material properties.

Table 4. Aluminum properties

Density	2719 kg m^{-3}
Specific heat	871 J $kg^{-1}K^{-1}$
Thermal conductivity	202.4 W $m^{-1}K^{-1}$

A constant temperature of 333 K was used on the outer wall of the heat sink in order to simulate the behavior of the heat exchanger and the melting of the material in one of the most extreme battery scenarios (Kim et al., 2019). The other external walls of the model were considered as adiabatic. Figure 4 shows the first configuration that is used and later parameterized for the generation of the other models with the dimensions and boundary conditions.

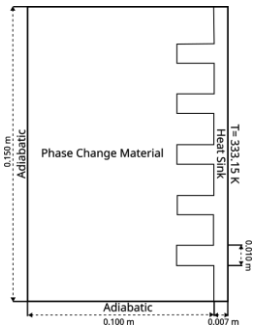

Figure 4. Heat exchanger computational domain and boundary conditions.

Although the geometry of the model is somewhat simple, the simulation of the phase change process of the material has several nonlinearities together with the presence of natural convection as a pushing force of the flow, therefore, a relatively small time step must be used to be able to correctly capture the physical phenomena in addition to the good quality of the computational mesh, since the temporal and spatial domain is extremely critical in this type of case. Fully structured meshes were generated with the orthogonal quality value equal to 1, representing the maximum quality for this parameter. The choice of structured meshes is due to the fact that it is possible to reduce diffusion phenomena between the elements. The table 5 shows the number of elements generated for each mesh. Table 6 shows the cases studied and the figure 5 illustrates the meshes used, where it is possible to see regions with greater refinements, because it is where there will be development of the boundary layer.

Table 5. Mesh size

Mesh	Number of elements
Case 1	46800
Case 2	40800
Case 3	52416

Table 6. Heat sink models.

Case	Fins	Length (m)
1	5	0.02
2	5	0.04
3	10	0.04

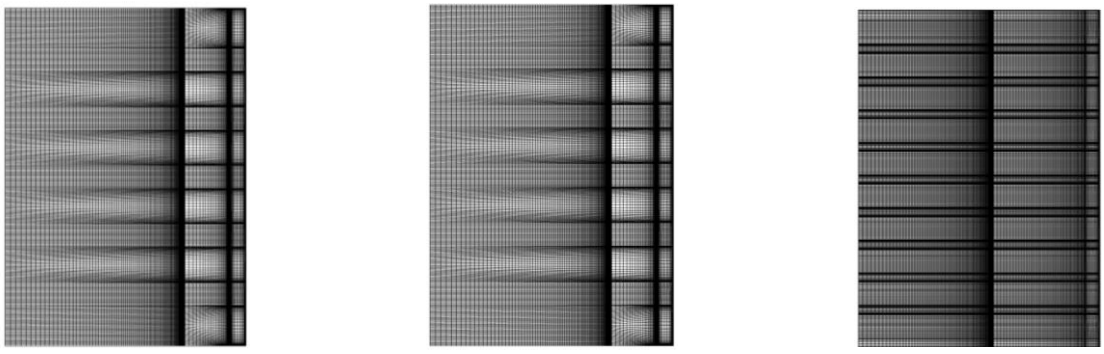

(a) (b) (c)

Figure 5. Computational meshes (a) case 1, (b) case 2, and (c) case 3.

3. RESULTS AND DISCUSSION

The transient simulations were generated with a total time of 1200s with a time step of 0.05s, in order to analyze the melting behavior of the material under critical conditions. Figure 6 illustrates the evolution of the liquid fraction for each case studied. Case 1 presents the lowest liquid fraction over the time studied with a value of approximately 14% of the molten material. Case 2 presents a similar behavior to case 1 with an almost linear evolution of the liquid fraction, however, with a higher liquid fraction of approximately 22%. Finally, case 3 presents the highest liquid fraction with approximately 24%, and a different behavior from the other cases, since it initially grows non-linearly with a profile close to an exponential, but after 250s it starts a profile closer to a linear behavior. This behavior represents a greater melting of the material in the initial instants of the simulation. Naturally, case 3 has a larger heat sink area due to the greater number of fins, and therefore presents a higher fraction of liquid within the initial minutes of the simulation.

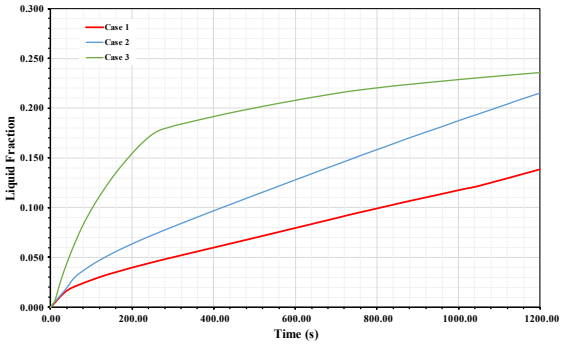

Figure 6. Liquid fraction over the time.

Although case 3 presents a higher liquid fraction in the initial minutes, the change in behavior of the melting material after 250s can be better understood by analyzing the contours of the liquid fraction in figure 7, where we can see that the areas on the sides of the fins present greater gradients of molten material, evidently, we can expect this behavior because it is expected that the temperature gradient is also greater in these regions considering that the heated wall faces form cavities with greater heat concentration. Therefore, analyzing the contour for case 3, we can observe that in 300s all the material in the region of this cavity generated has already been melted, therefore, the region of greater heat concentration for this model is quickly filled by the smaller area to the detriment of the physical characteristics of this geometry. Case 2 presents a good configuration, since after 1200s there is still considerable space for melting in the region between the fins, despite less solidification in the given time, it can overtake case 3 in a larger analysis.

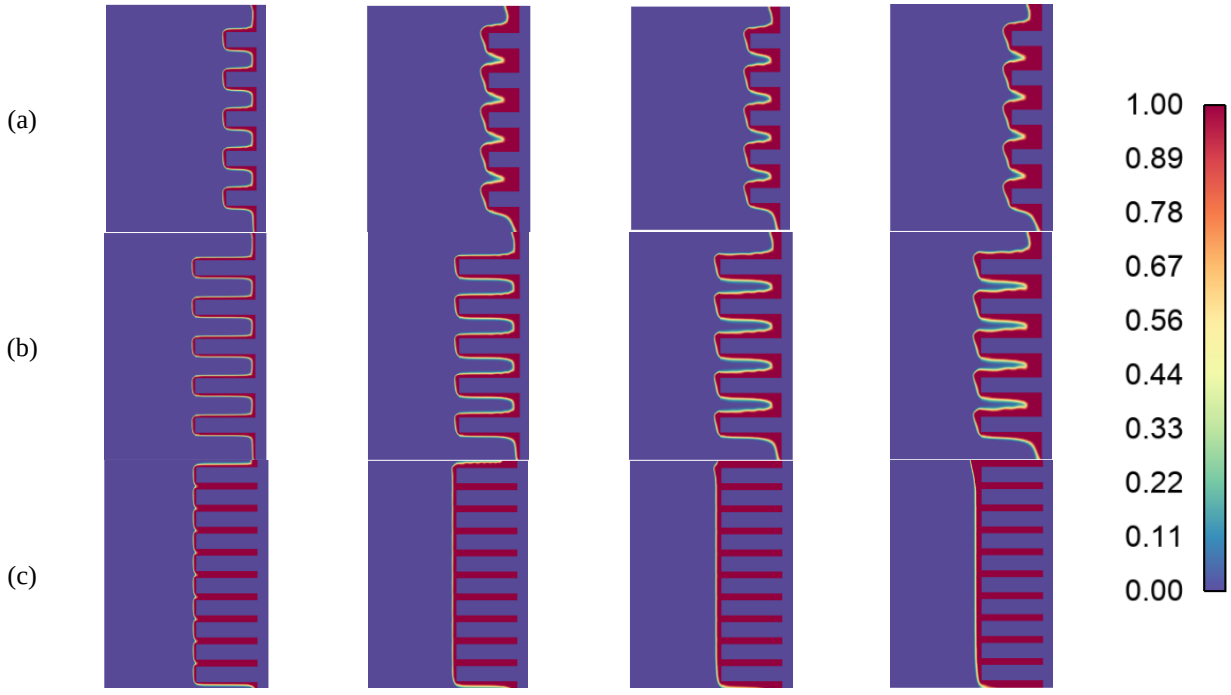

Figure 7. Transient liquid fraction contour for (a) Case 1, (b) Case 2 and (c) Case 3.

In figure 7, we can analyze that the liquid fraction profile does not occur as a diffusion in one direction, but with the generation of several layers between the fins that join along the time. We can understand these effects as a consequence of natural convection in the domain, a fact that brings non-linearities in the problem, but that can contribute to the heat transfer process. We can use the Rayleigh number to understand the relationship between the inertial forces and the buoyancy forces in order to verify the influence of natural convection in the cases studied. Figure 8 shows the behavior of the Rayleigh number over time, where we can observe that the values obtained are generally higher than 10^8 after the initial seconds of the simulation. In this type of problem, as the boundary layer appears and the thickness of the melt layer increases, the conductive heat transfer decreases, as a result of the decrease of the thermal gradient and the reduced conductivity of the liquid phase of the PCMs (Mallya & Haussener, 2021). As we work with the average temperature in the melting zone of the material, there is a reduction in the temperature variation of the solid and the PCM zone, which leads to the Rayleigh number profile showing a reduction profile.

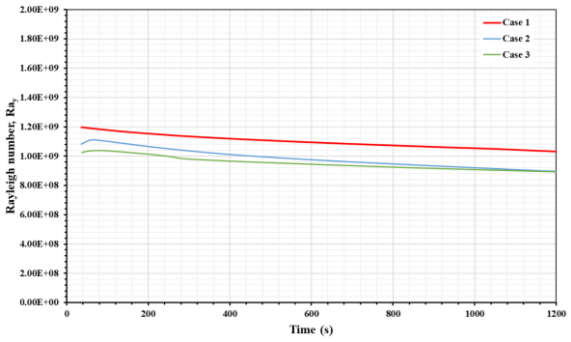

Figure 8. Rayleigh number over time.

Figure 9 shows the velocity contour of the liquid fraction generated by the melting process. Several boundary layer zones can be observed at the expense of the geometry of the fins, in addition, we can analyze that in this type of problem we will have two thermal boundary layers to form: one next to the hot wall and one next to the cooler melt interface, initiating the mixed conduction-convection regime. This result is very important because it indicates that the presence of the fins allows the generation of several boundary layers that generate recirculation zones when they meet and that interrupt the development of the flow. This type of behavior is more evident in cases 1 and 2 throughout the period, however, in case 3 the presence of these phenomena is reduced due to the small size of the cavities between the fins, where we can observe that initially at 600s we have two parallel boundary layers that meet, and at the end of the simulation at 1200s, there is only one boundary layer profile generated in front of the fins with the smaller cavities already completely filled with material.

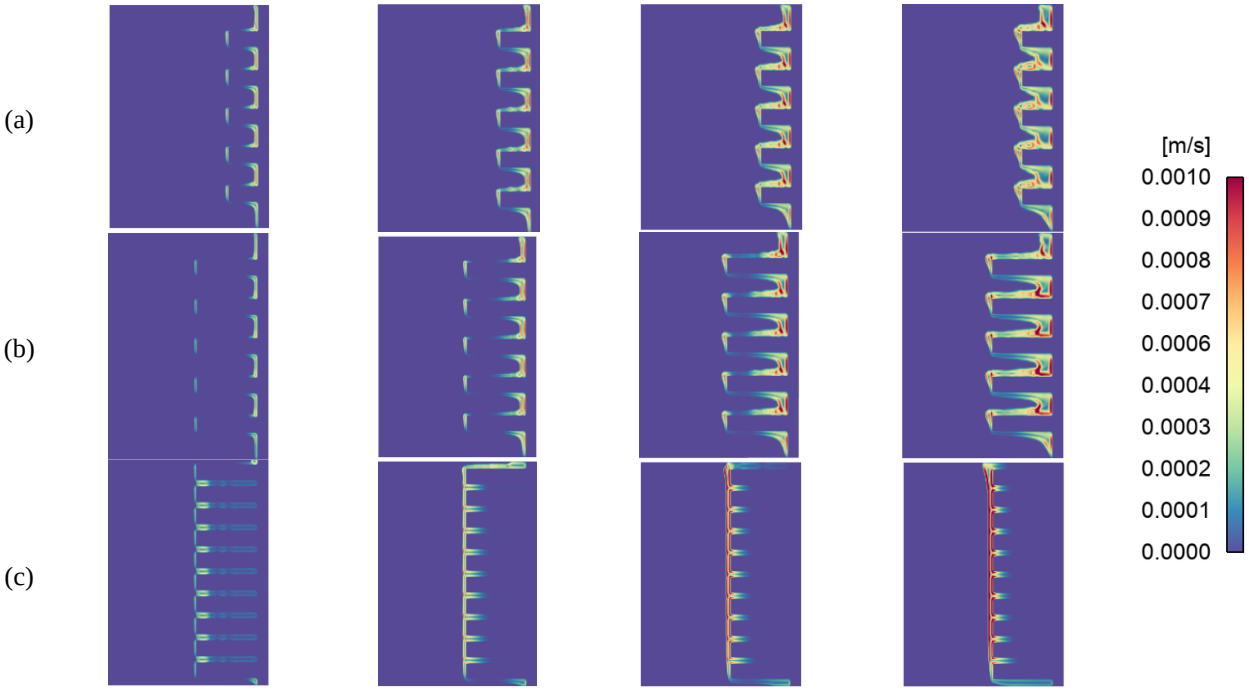

Figure 9. Velocity contours for (a) Case 1, (b) Case 2 and (c) Case 3.

In figure 10 it is possible to analyze contours of the temperature profile of the cases. The temperature profile of the solid evolves rapidly due to the conduction process in aluminum, however, the heat transfer process to melt the PCM material occurs more slowly due to the properties of the material. Physically analyzing the phenomena, we were able to verify several temperature gradients in the region of the fins, especially in cases 1 and 2 where the number of fins is lower, and consequently, greater cavity space between them for melting the material. As the simulation time evolves, it is possible to observe that the temperature gradients by convection evolve in a similar way to the Kelvin-Helmholtz instabilities, and several layers are formed due to the shear flows of the thermal boundary layers near the wall and the melting solid. In case 3 the melting of the material is limited after the melting of the material between the fins to a thermal boundary layer with few unstable temperature gradients, and the process is limited compared to the previous cases.

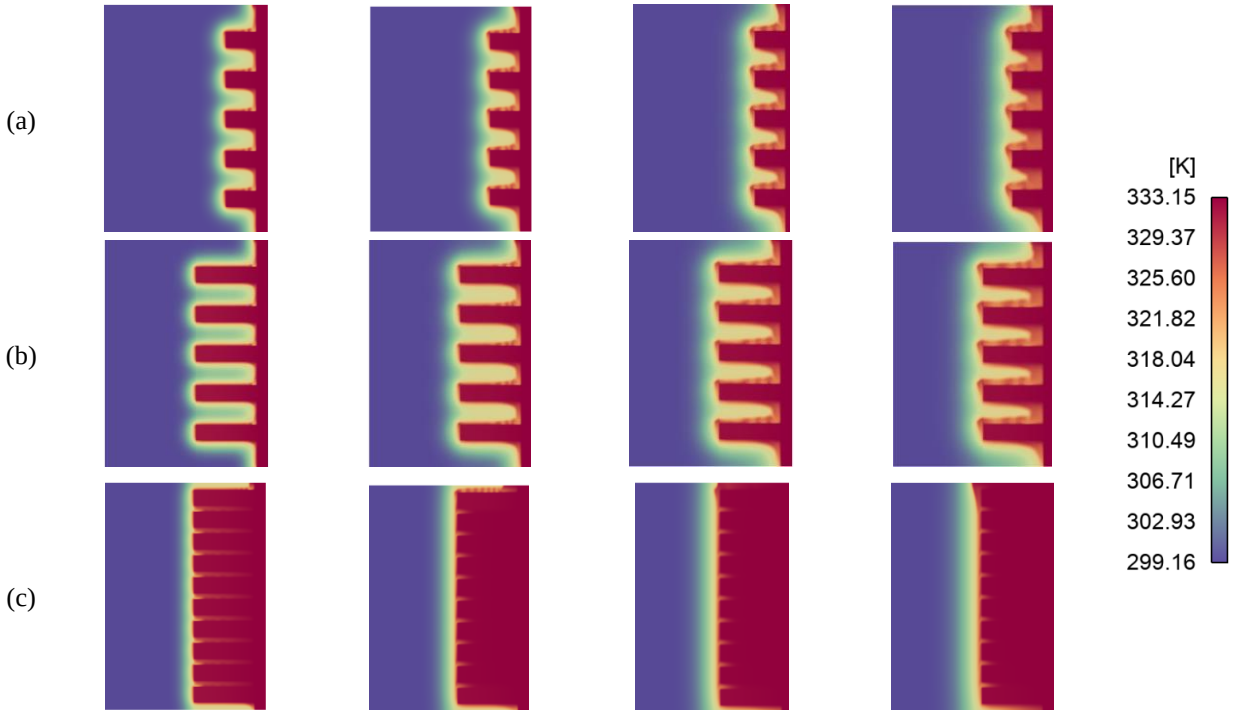

Figure 10. Temperature contours for (a) Case 1, (b) Case 2 and (c) Case 3.

For case 3 after the complete melting of the material between the fins, there is a thermal boundary layer with few unstable temperature gradients, and the process is limited compared to the previous cases. In figure 11 we can check the Nusselt number, which helps us to analyze the influence of these differences of configurations on the heat transfer process. The values are higher at the beginning of the simulation due to the large gradients of heat flux in the wall, since the case works with a prescribed temperature. An interesting result is that both case 1 and case 2 present globally higher values than case number 3, although the latter presents higher liquid fraction value at the beginning of the simulation. This result is important because it is inherent to the fin configuration and may indicate that a smaller number of fins in the domain allows greater heat transfer with the emergence of several distinct boundary layers inside the PCM zone. The configuration of case 2 presents better results and shows that the variation of the fin length is also a considerable factor.

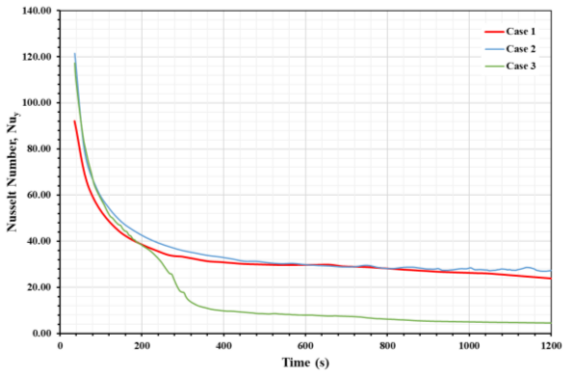

Figure 11. Nusselt number over time.

It is possible to analyze the behavior of the thermal storage capacity during the analysis time in figure 12. Case 2 again shows a better behavior with an almost linear growth, surpassing case 3 after 1000s of simulation, again this configuration proved to be better with greater storage capacity over time, although for a short period the configuration can be interesting because it can quickly absorb a certain amount of heat. Case 1 shows a lower behavior than the others.

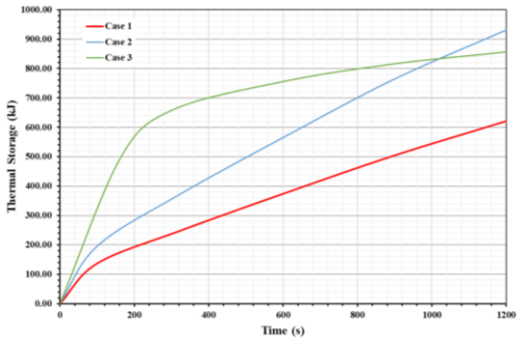

Figure 12. Thermal storage over time.

The liquid fraction does not represent as a direct comparison the amount of melting of the material in the cases, because the PCM area of each case is different, therefore, we can correlate the density of the melted material with the volume and obtain the total mass of liquid over time. Figure 13 demonstrates the mass of molten material, and we can notice that the behavior is directly proportional to the storage capacity. Thus, again case two was superior and produced higher amount of liquid mass.

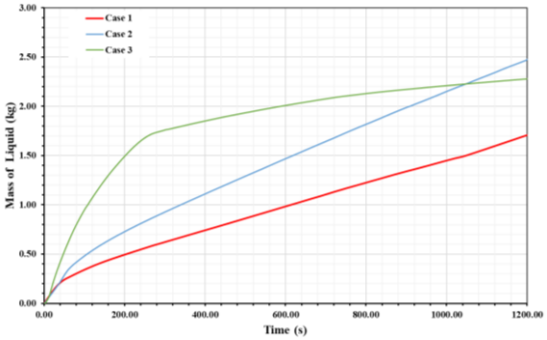

Figure 13. Mass of liquid over time.

4. CONCLUSION

The presence of the finned heat sink in the heat exchanger proved to be efficient, considering that the presence of several zones with boundary layer development provided intensification of heat transfer mainly where these phenomena were more evident. The presence of a larger number of fins in the heat exchanger reduced the performance of the equipment over time in relation to the thermal storage capacity and the mass of molten liquid produced. In this study, the fin thickness was considered as constant, but it should be a variable parameter in a next study, considering that the cavity zone between the fins proved to be extremely important in the performance of the heat exchanger.

Natural convection was strongly present in the analysis, and the instabilities generated during the development of the thermal boundary layer were also shown to be positive in the heat transfer process, considering that due to the profile of the geometry of the fins, the development of the boundary layers was constantly interrupted, a fact that is also inherent to the regions of cavities formed in the zones between the fins.

Although for an electric vehicle it is interesting to absorb a greater amount of heat in a short period of time, case 2 proved to be more promising, as it manages to maintain a good relationship between the amount of heat absorption and melting time in relation to case 3 that despite being able to melt a greater amount of material in a short period of time, its performance reduces rapidly.

In a next analysis, an optimization of the fin length can be considered to find a global optimal configuration with the aim of trying to find a higher performance of the heat exchanger in relation to the studied cases.

5. REFERENCES

Bicer, Y., & Dincer, I. (2017). Comparative life cycle assessment of hydrogen, methanol and electric vehicles from well to wheel. *International Journal of Hydrogen Energy*, *42*(6), 3767–3777. https://doi.org/10.1016/j.ijhydene.2016.07.252

Gau, C., & Viskanta, R. C. (1986). *Melting and solidification of a pure metal on a vertical wall*.

Helbling, M., & Meierrieks, D. (2022). Global warming and urbanization. *Journal of Population Economics*. https://doi.org/10.1007/s00148-022-00924-y

Heyhat, M. M., Mousavi, S., & Siavashi, M. (2020). Battery thermal management with thermal energy storage composites of PCM, metal foam, fin and nanoparticle. *Journal of Energy Storage*, *28*. https://doi.org/10.1016/j.est.2020.101235

Javani, N., Dincer, I., Naterer, G. F., & Rohrauer, G. L. (2014). Modeling of passive thermal management for electric vehicle battery packs with PCM between cells. *Applied Thermal Engineering*, *73*(1), 307–316. https://doi.org/10.1016/j.applthermaleng.2014.07.037

Kamkari, B., Shokouhmand, H., & Bruno, F. (2014). Experimental investigation of the effect of inclination angle on convection-driven melting of phase change material in a rectangular enclosure. *International Journal of Heat and Mass Transfer*, *72*, 186–200. https://doi.org/10.1016/j.ijheatmasstransfer.2014.01.014

Kim, J., Oh, J., & Lee, H. (2019). Review on battery thermal management system for electric vehicles. In *Applied Thermal Engineering* (Vol. 149, pp. 192–212). Elsevier Ltd. https://doi.org/10.1016/j.applthermaleng.2018.12.020

Liu, W., Placke, T., & Chau, K. T. (2022). Overview of batteries and battery management for electric vehicles. *Energy Reports*, *8*, 4058–4084. https://doi.org/10.1016/J.EGYR.2022.03.016

Luo, J., Zou, D., Wang, Y., Wang, S., & Huang, L. (2022). Battery thermal management systems (BTMs) based on phase change material (PCM): A comprehensive review. In *Chemical Engineering Journal* (Vol. 430). Elsevier B.V. https://doi.org/10.1016/j.cej.2021.132741

Mallya, N., & Haussener, S. (2021). Buoyancy-driven melting and solidification heat transfer analysis in encapsulated phase change materials. *International Journal of Heat and Mass Transfer*, *164*. https://doi.org/10.1016/j.ijheatmasstransfer.2020.120525

Pesaran, A., Keyser, M., & Burch, S. (1999). *An approach for designing thermal management systems for electric and hybrid vehicle battery packs*. National Renewable Energy Laboratory, Golden, CO (US).

Sanguesa, J. A., Torres-Sanz, V., Garrido, P., Martinez, F. J., & Marquez-Barja, J. M. (2021). A review on electric vehicles: Technologies and challenges. In *Smart Cities* (Vol. 4, Issue 1, pp. 372–404). MDPI. https://doi.org/10.3390/smartcities4010022

Schoewel, F., & Hochgeiger, E. (2014). The high-voltage batteries of the BMW i3 and BMW i8. *Proceedings of the Advanced Automotive Battery Conference (AABC), Atlanta, GA, USA*, *45*.

Shokouhmand, H., & Kamkari, B. (2013). Experimental investigation on melting heat transfer characteristics of lauric acid in a rectangular thermal storage unit. *Experimental Thermal and Fluid Science*, *50*, 201–212. https://doi.org/10.1016/j.expthermflusci.2013.06.010

Voller, V. R., Brent, A. D., & Prakash, C. (n.d.). *Modelling the mushy region in a binary alloy*.

Voller, V. R., & Prakash, C. (1987). A fixed grid numerical modelling methodology for convection-diffusion mushy region phase-change problems. *International Journal of Heat and Mass Transfer*, *30*(8), 1709–1719.

Zeng, L., Lu, J., Li, Y., Li, W., Liu, S., & Zhu, J. (2017). Numerical study of the influences of geometry orientation on phase change material's melting process. *Advances in Mechanical Engineering*, *9*(10). https://doi.org/10.1177/1687814017720084

Zhang, X., Li, Z., Luo, L., Fan, Y., & Du, Z. (2022). A review on thermal management of lithium-ion batteries for electric vehicles. *Energy*, *238*. https://doi.org/10.1016/j.energy.2021.121652

6. RESPONSIBILITY NOTICE

The author(s) is (are) the only responsible for the printed material included in this paper.